Hypersonic Merged-Layer Flow on a Sphere

A. C. Jain*
NASA Langley Research Center, Hampton, Virginia

A two-term series solution of the full Navier-Stokes equations with slip and temperature jump surface conditions has been obtained for a merged-layer (ML) flow in the fore region of a sphere. Downstream effects due to the elliptic nature of the equations, which allow upstream propagation of the disturbances and the spherical asymmetry of the ML edge with the spherical surface, have been incorporated in the analysis. Equations determining the coefficients of the series expansion have been integrated numerically from the surface to the freestream so as to capture the shock-wave-like structure as part of the computational domain. When the downstream effects were included in the analysis, stagnation point heat-transfer coefficient C_H and skin-friction coefficient C_F were reduced and the results came closer to the experimental data of Boylan and the direct-simulation Monte Carlo (DSMC) results of Moss and Bird. It was found that the downstream effects significantly affected stagnation point flow characteristics for the Knudsen number >0.08. Comparison of the results of C_H and pressure ratio ($p/p_{\text{stagnation}}$) on the spherical surface with the available experimental data indicated the validity of the present formulation up to $\theta \approx 30$ deg. Rarefaction effects on the pressure distribution become important only in the very low range of Reynolds numbers. Present results predict a flow structure in the outer part of the ML significantly different from the DSMC calculations, while the overall surface characteristics of the flow are in reasonable agreement with the DSMC results up to an altitude of 109.75 km under Shuttle flight conditions.

Nomenclature

a_∞ = freestream speed of sound
C_F = skin-friction coefficient, $\tau/0.5\rho_\infty U_\infty^2$
C_H = heat-transfer coefficient, $\dot{q}/0.5\rho_\infty U_\infty^3$
C_p = specific heat at constant pressure
C_v = specific heat at constant volume
K = coefficient of thermoconductivity
Kn = Knudsen number
K_r^2 = Cheng's correlation parameter
M_∞ = freestream Mach number, U_∞/a_∞
$\tilde{n}_{e0}$ = $\tilde{r}_{e0} - 1$, merged layer thickness at stagnation point
p = pressure
Pr = Prandt number, $\mu C_p/K$
$\dot{q}$ = heat flux
r = radius vector measured from the center of a sphere
r_B = nose radius
$\tilde{r}_{e0}$ = merged-layer outer edge at stagnation point
Re = Reynolds number, $\rho_\infty U_\infty r_B/\mu(T_{0\infty})$
Re_∞ = freestream Reynolds number, $\rho_\infty U_\infty \delta_X r_B/\mu(T_\infty)$
T = temperature
u,v = velocity components in r and θ directions, respectively
α = thermal accommodation coefficient
γ = specific heat ratio, C_p/C_v
θ_2 = spherical asymmetry parameter defined in Eq. (5)
θ,η = transformation defined in Eq. (5)
Θ = angle the radius vector makes with the axis of symmetry
Λ = $\frac{1}{2} + 1/[(\gamma-1)M_\infty^2]$
μ = coefficient of viscosity
ρ = density
σ = momentum accommodation coefficient
τ = skin friction

Subscripts and Superscripts

b = value at the base of viscous layer
e = value at the merged-layer outer edge
w = value at the wall
0∞ = freestream stagnation value
∞ = value in freestream
$(\bar{\ })$ = dimensionless value
$(\ )'$ = differentiation with respect to η

Introduction

An aeroassisted orbital transfer vehicle is expected to fly in the higher region of the atmosphere for a sustained period of time so as to achieve the desired reduction in velocity by aerodynamic forces. If the vehicle is designed for a low ballistic coefficient, this aeroassist maneuver will occur in the transitional regime.[1] Here, a merged layer (ML) is formed around the space vehicle and its flow characteristics can be investigated on the basis of the full Navier-Stokes (NS) equations with slip and temperature jump surface conditions. The Navier-Stokes equations are elliptic in nature and thus permit the propagation of disturbances from several sources to the upstream region of the body. We shall term these disturbances as downstream effects.

Levinsky and Yoshihara[2] were the first to solve the stagnation point ML flow on the basis of the thin-layer approximation of the NS equations with no-slip conditions. They found that the impact pressure decreased with the decrease in Reynolds number, which was contrary to the trend of impact pressure data of Potter and Bailey.[3] They attributed this failure to the no-slip conditions in their analysis. Jain and Adimurthy[4] introduced slip into the analysis of Ref. 2 and found that the impact pressure decreased further due to slip. Jain and Adimurthy[4] improved upon the analysis by considering the full NS equations and again developed local similar solutions with surface slip conditions, but neglecting the downstream effects. Consistent with the experimental data of Potter and Bailey,[3] the results indicated an increase of stagnation point impact pressure as the Reynolds number

Presented as Paper 85-1031 at the AIAA 20th Thermophysics Conference, Williamsburg, VA, June 19-21, 1985; revision received Feb. 28, 1986.

*National Research Council Senior Research Associate, Aerothermodynamics Branch, Space Systems Divison (on leave from Indian Institute of Technology, Kanpur, India).

decreased. Detailed comparisons with other theoretical and experimental investigations led us to believe that the Navier-Stokes equations can give reliable results beyond the theoretically permissible limits of validity of the continuum approach. In Ref. 5, we made further detailed comparisons with viscous shock layer results and the direct-simulation Monte Carlo (DSMC)) calculations of Bird.[6] We found reasonably good agreement of the heat-transfer coefficient C_H with the DSMC predictions up to a Knudsen number of 0.6. Kumar and Jain[7] incorporated in the analysis of Ref. 4 the real-gas effects due to nonequilibrium dissociation with no-slip surface conditions. Henrick[8] introduced slip conditions in the analysis of Ref. 7 and found reasonably good agreement between the prediction of stagnation point heat-transfer coefficient C_H and the experimental data of Scott.[9]

Davis[10] simplified the NS equations by retaining terms up to second order in the inverse square root of the Reynolds numbers. The resulting equations, referred to as the viscous shock layer (VSL), are uniformly valid in the entire shock layer between the body and the shock. These governing equations are parabolic in nature and thus do not permit computation of the upstream propagation of disturbances in the flow. Davis[10] further calculated the VSL flow on a blunt body by retaining the variation of the VSL thickness. Kaiser and Flügge-Lots[11] solved the same set of the governing equations by a two-term asymptotic series expansion and retained only the effect of the VSL thickness variation. They found that the local similar analysis, neglecting variation of the VSL thickness, can lead to substantial errors in the results. Assuming the spherical symmetry of the VSL outer edge with the body surface, Kuo[12] investigated the stagnation point flow on the basis of the two-term series solution of the full NS equations. Due to the elliptic nature of the equations, second-order terms representing upstream propagation of disturbances appear in the equations determining the coefficients of the leading term. He evaluated second-order effects by an iterative process and found that these terms contribute negligibly to the leading term of the series expansion. We may point out that the downstream effects represented by the ML or the VSL thickness variation and the upstream propagation of disturbances appear in the equations determining the zeroth- and second-order terms in nonlinear and coupled manner. Hence, in case we determine one effect and suppress the other, the results may not correctly estimate its contribution.

In the present investigation, a two-term series solution of the full Navier-Stokes equations with surface slip and temperature jump conditions for the ML flow on a sphere has been obtained. The analysis incorporates the downstream effects due to the ML thickness variation and the upstream propagation of the disturbances in the stagnation zone. Attempts have been made to assess the downstream effects in the stagnation zone, to assess the accuracy and range of validity of the two-term solution, and to assess the areas of agreement between the present predictions and the DSMC calculations. We achieve these objectives by solving the zeroth- and second-order equations iteratively and comparing the results with the available theoretical investigations and the experimental data. A parametric study has been carried out with a view to understanding the salient features of low-density flows.

Mathematical Formulation of the Problem

The full Navier-Stokes equations in a spherical-polar coordinate system with axial symmetry are nondimensionalized as follows:

$$\bar{u}=\frac{u}{U_\infty},\quad \bar{v}=\frac{v}{U_\infty},\quad \bar{p}=\frac{p}{\rho_\infty U_\infty^2},\quad \bar{\rho}=\frac{\rho}{\rho_\infty}$$

$$\bar{T}=\frac{T}{T_{0\infty}},\quad \bar{\mu}=\frac{\mu}{\mu(T_{0\infty})},\quad \bar{r}=\frac{r}{r_B} \tag{1}$$

Slip and temperature jump conditions on the surface are[13]

$$\bar{u}_b=A\cdot\frac{M_\infty}{Re}\cdot\sqrt{\frac{T_\infty}{T_{0\infty}}}\cdot\frac{\mu}{\bar{\rho}\sqrt{\bar{T}}}\left(\frac{\partial\bar{u}}{\partial\bar{r}}-\frac{\bar{u}}{\bar{r}}\right)_{\bar{r}=1}$$

$$\bar{v}_b=0$$

$$\bar{T}_b=\bar{T}_w+B\cdot\frac{M_\infty}{RePr}\cdot\sqrt{\frac{T_\infty}{T_{0\infty}}}\cdot\frac{\bar{\mu}}{\bar{\rho}\sqrt{\bar{T}}}\left(\frac{\partial\bar{T}}{\partial\bar{r}}\right)_{\bar{r}=1} \tag{2}$$

where

$$A=\sqrt{\frac{\pi\gamma}{2}}\cdot\frac{2-\sigma}{\sigma}$$

and

$$B=\sqrt{\frac{\pi\gamma}{2}}\cdot\frac{2-\alpha}{\alpha}\cdot\frac{2\gamma}{\gamma+1}$$

For the no-slip case,

$$\bar{u}=\bar{v}=0 \text{ and } \bar{T}=\bar{T}_w \text{ at } \bar{r}=1 \tag{3}$$

The boundary conditions in the freestream are

$$\bar{u}=\sin\theta,\quad \bar{v}=-\cos\theta,\quad \bar{\rho}=1$$

$$\bar{p}=1/\gamma M_\infty^2,\quad \bar{T}=1-(1/2\Lambda) \tag{4}$$

where

$$\Lambda=\tfrac{1}{2}+1/(\gamma-1)M_\infty^2$$

Using the following transformation of independent variables, the physical flow domain is transformed into a rectangular computational domain:

$$\theta=\theta,\quad \eta=(\bar{r}-1)/(\bar{r}_e-1) \tag{5}$$

where

$$\bar{r}_e=\bar{r}_{e0}+\eta_2\sin^2\theta$$

Here, $\bar{r}_{e0}$ specifies the merged-layer outer edge at the stagnation point and η_2 is the parameter that signifies the extent of variation of the ML thickness on the sphere from its value at the stagnation point. Both $\bar{r}_{e0}$ and η_2 are to be obtained as part of the computational procedure.

Consistent with the form of the boundary conditions, the symmetry conditions about the axis and the fact that the Rankine-Hugoniot pressure behind a shock wave and the Newtonian pressure on the surface vary as $\sin^2\theta$, we assume the following form of series expansions for the various flow variables:

Zeroth Order	Second Order
$\bar{u}(\eta,\theta)=u_0(\eta)\sin\theta$	$+u_2(\eta)\sin^3\theta+\ldots$
$\bar{v}(\eta,\theta)=v_0(\eta)\cos\theta$	$+v_2(\eta)\cos\theta\sin^2\theta+\ldots$
$\bar{\rho}(\eta,\theta)=\rho_0(\eta)$	$+\rho_2(\eta)\sin^2\theta+\ldots$
$\bar{p}(\eta,\theta)=p_0(\eta)+p_2(\eta)\sin^2\theta$	$+p_4(\eta)\sin^4\theta+\ldots$
$\bar{T}(\eta,\theta)=T_0(\eta)$	$+T_2(\eta)\sin^2\theta+\ldots$

(6)

Substituting the various expansions of the flow variables into the governing equations and the boundary conditions and collecting terms of like powers of θ, we get ordinary differential equations and the boundary conditions for the various order terms in Eq. (6). The leading zeroth-order term imposes

a spherical symmetry (local similarity) on the flow, but is accurate in the immediate vicinity of the stagnation point. Inclusion of the second-order term removes the locally similar restriction and extends the range of the solution validity to distances further downstream of the stagnation point.

A typical zeroth-order equation is of the form: $F(u_0,...u_2, v_2,..., \bar{r}_{e0}, \eta_2)=0$. Mathematically, the second-order terms (viz, u_2, v_2, η_2) in the zeroth-order equation arise due to the elliptic nature of the governing equations and the asymmetry in the boundary conditions and represent corrections in the zeroth-order equation. Physically, the presence of the second-order terms in the zeroth-order equation allow the stagnation point solution to realize what is happening further downstream. Terms like u_2, v_2, etc., represent the upstream propagation of disturbances from the downstream region of the validity of solution. The parameter η_2 called here, for lack of a better name, a spherical asymmetry parameter because it arises due to the departure of the presumed outer merged-layer surface from the spherical surface. These two effects, viz, the upstream propagation of disturbances in the stagnation zone and the spherical asymmetry of the ML outer surface, are termed here as downstream effects. These two effects appear in the zeroth-order equations in a large number of nonliner and coupled terms. Hence, evaluating one effect and suppressing the other may lead to incorrect results. Details of the calculations are given in Ref. 14.

Numerical Method of Integration

First-order derivatives are replaced by central differences in the zeroth- and second-order momentum and the energy equations. Endpoint derivatives are replaced by three-point differencing. The resulting algebraic equations at the various grid points are solved by the method of accelerated successive replacement. The continuity equation determines the density and is integrated from the ML outer edge toward the surface by trapezoidal, Simpson's, and Weddle's rules. It should be noticed that the derivative of the density, $(\partial\rho/\partial\eta)_{\text{wall}}$, becomes singular at the surface unless

$$\frac{\partial\bar{v}}{\partial\eta} = -2n_e\bar{u} \text{ for the slip case}$$
$$= 0 \text{ for the no-slip case} \qquad (7)$$

Equation (7) is used to evaluate the asymmetry parameter η_2. Equation (7) was first used by Ho and Probstein[15] in determining the stagnation point viscous shock layer thickness and later several investigators used Eq. (7) in determining different quantities. Instead of using L'Hospital's rule twice in the evaluation of $(\partial\rho/\partial\eta)_{\text{wall}}$, the density at the wall is obtained from the equation of state. The normal momentum equation is evaluated on the surface to give $(\partial\bar{p}/\partial\eta)_{\text{wall}}$ and then the pressure at the wall is given by

$$\bar{p}(1)=\bar{p}(2)-\Delta\eta\left(\frac{\partial\bar{p}}{\partial\eta}\right)_{\text{wall}}$$

The stagnation point ML thickness $\bar{n}_{e0}$ is evaluated from the zeroth-order equations by imposing the condition that the flow variables approach the outer edge conditions asymptotically.

For a prescribed value of η_2, equations for the zeroth and second orders are solved to a specified degree of accuracy. The results so obtained are used in the second and successive iterations between the zeroth- and second-order equations until convergence is achieved. It was found that, after three global iterations, the surface characteristics did not differ up to three decimal places. We further observed that, for prescribed conditions, $(\partial v_0/\partial\eta)_{\text{wall}}\approx 0$ in all of the cases considered and that the values of $(\partial v_2/\partial\eta)_{\text{wall}}$ vary almost linearly with η_2. In the initial stages of computation, two values of η_2 are chosen to give the slope of the curve of $(\partial v_2/\partial\eta)$ vs η_2. This curve is extended to cross the η_2 axis. The value of η_2 at the η_2 axis so obtained is taken in the next global iteration, and it gave $(\partial v_2/\partial\eta)_{\text{wall}}\approx 0.0$. Once converged results are obtained for a particular value of Reynolds number, these results are used as initial values for the next Reynolds number.

Discussion of Results

In Figs. 1-4, we have drawn various characteristics of stagnation point flow with and without the downstream effects. Figure 1 shows that the downstream effects increase the ML thickness and decrease the maximum temperature and tangential component of velocity inside the merged layer. Figure 2 gives the variation of the spherical asymmetry parameter η_2 and of the stagnation point ML thickness with and without the downstream effects against the Reynolds number. We found that, as the Reynolds number decreased, the value of the parameter η_2 increased. Also, the downstream effects increased the values of the stagnation point ML thickness from its value without the downstream effects. Figures 3 and 4 indicate that the heat-transfer coefficient C_H and the skin-friction coefficient $C_F/\sin\theta$ decrease in value as a result of introducing the downstream effects. The curves of C_H and $C_F/\sin\theta$ with and without the downstream effects merge smoothly at a Knudsen number (Kn) of 0.08. The difference in their values increases with increase in the values of Kn. Downstream effects decrease $C_F/\sin\theta$ more than C_H. Figure 5 shows that the predicted values of C_H with downstream effects plotted against K^2 (Cheng's correlating parameter) are closer to the experimental data of Boylan[16]

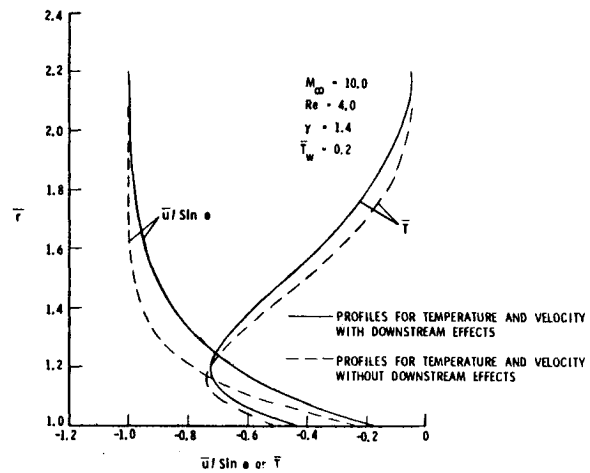

Fig. 1 Stagnation point temperature and velocity profiles with and without downstream effects.

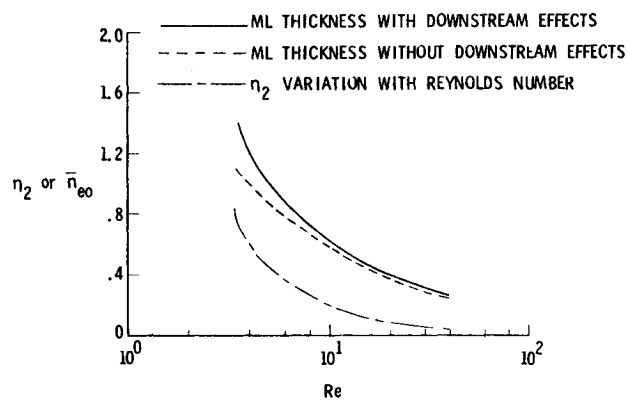

Fig. 2 Variation of stagnation point ML thickness with and without downstream effects and asymmetry parameter n_2 vs Reynolds number.

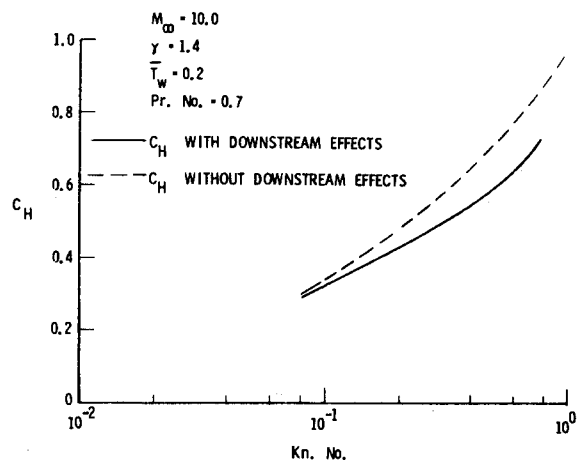

Fig. 3 Variation of stagnation point heat-transfer coefficient C_H with and without downstream effects vs Knudsen numbers.

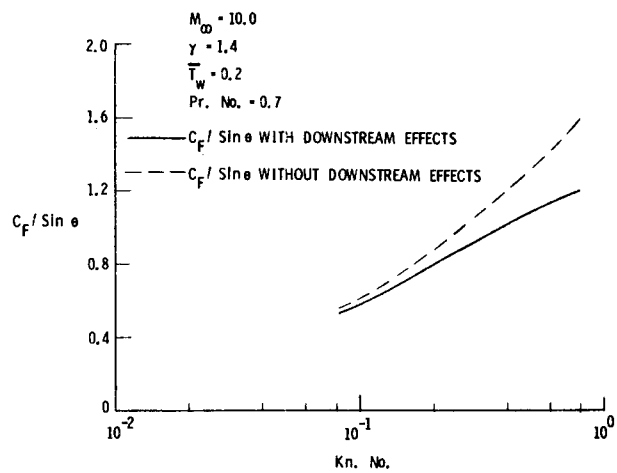

Fig. 4 Variation of stagnation point skin-friction coefficient with and without downstream effects vs Knudsen numbers.

than the values of C_H obtained without the downstream effects.

In Figs. 6 and 7, we have compared the results of the heat-transfer coefficient C_H and the pressure ratio $(p/p_{\text{stagnation}})$ on the surface of the sphere from our present solution with the available theoretical calculations and the experimental data. The purpose of the comparison is to establish the accuracy and range of the validity of the two-term approximation. Figure 6 gives the comparison of C_H with the arcjet data[9] on the non-catalytic wall of the sphere. We noticed that 1) the zeroth-order solution gave a constant value of the heat flux $\dot{q}$ over the spherical surface, while the two-term solution gave the variation of $\dot{q}$ with the distance downstream of the stagnation point and 2) the two-term solution gave results in reasonably good agreement with Scott's[9] data up to $\theta = 35$ deg. We further noticed that the experimental data were for real-gas effects present in the flow, while the present calculations were based upon ideal-gas assumption. Henrick[8] introduced the slip velocity, temperature, and concentration jump conditions on the surface with the real-gas effects in the analysis of Kumar and Jain.[7] We found that the difference in the predictions of the stagnation point heat flux $\dot{q}$ with and without the real-gas effects was negligibly small, indicating a small contribution of the real-gas effects on $\dot{q}$ under the conditions present in the arcjet facility of the NASA Johnson Space Center. Calculations of the pressure ratios $(p/p_{\text{stagnation}})$ for $M_\infty = 5.4$, $\gamma = 5/3$, $Re = 27$, $\bar{T}_w = 0.1$, $Pr = 0.7$ and $M_\infty = 6.3$, $\gamma = 5/3$, $Re = 90$, $\bar{T}_w = 0.1$, $Pr = 0.7$ have been made. The two sets of prescribed conditions correspond to the lowest and the highest values of

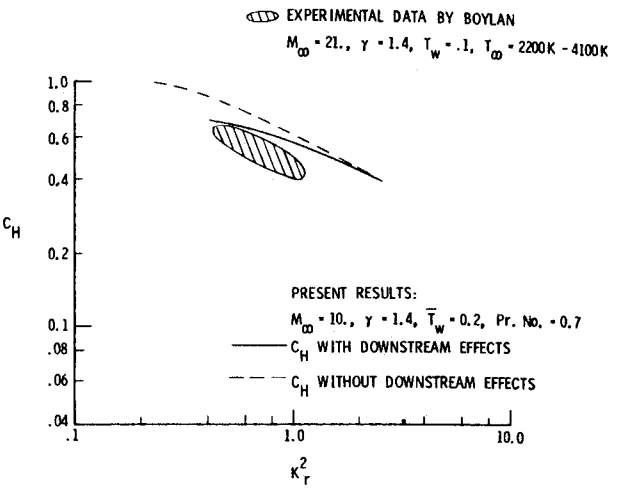

Fig. 5 Comparison of stagnation point C_H with and without downstream effects with experimental data of Boylan.

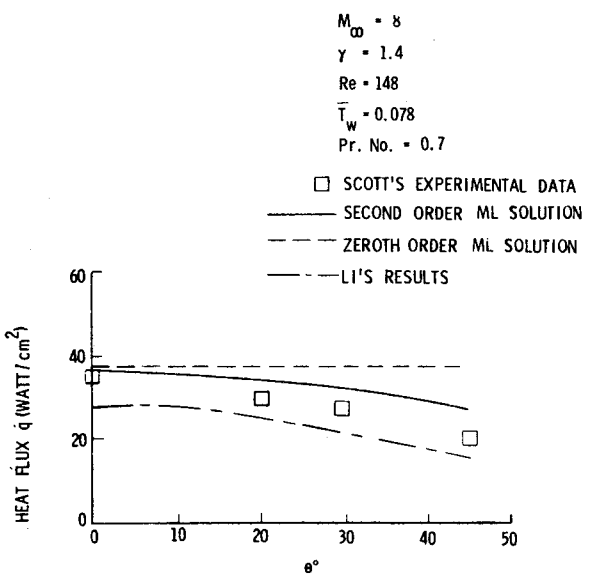

Fig. 6 Comparison of stagnation point heat flux with experimental data of Scott.

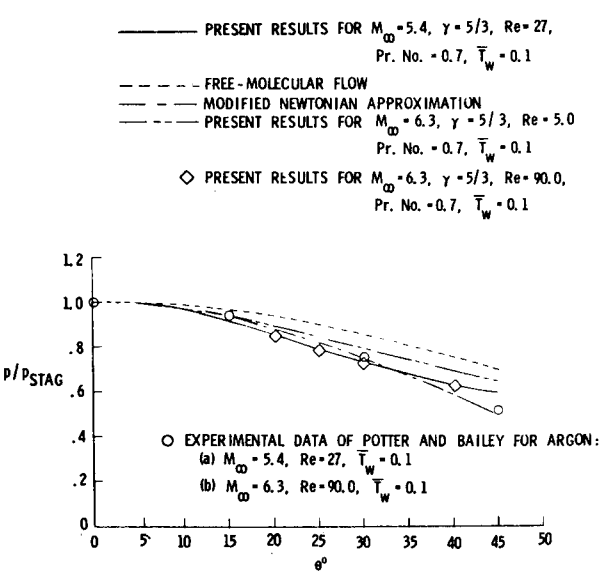

Fig. 7 Comparison of pressure distribution over a sphere from the present calculations and other theoretical and experimental investigations.

the Reynolds numbers found in Potter and Bailey's[3] experimental data on argon. From Fig. 7, we found that the theoretical curves for $Re=27$ and 90 coincided, that the experimental data for $Re=27$ and 90 coincided, and that the theoretical and experimental data agreed among themselves and with the modified Newtonian approximation with a reasonable degree of accuracy up to $\theta=30$ deg. Also we noticed that the curve for $(p/p_{\text{stagnation}})$ for $Re=5.0$ shifted toward the free molecular curve for the pressure ratio. This led us to conclude that, for moderate Reynolds numbers (>27.0), a modified Newtonian approximation might predict the surface pressure distribution, while for low Reynolds numbers (≈ 5.00), rarefaction effects become important on the pressure distribution. To assess the accuracy of the present formulation, the results of the two-term solution were substituted in the tangenital momentum and energy equations. It was found that the present solution satisfied both equations with a reasonable degree of accuracy up to $0=30$ deg.

Vogenitz and Takata[17] carried out DSMC calculations for a monatomic gas with a hard-sphere model. In the present investigation, we have tried to simulate the conditions of DSMC calculations as closely as is possible. Detailed results are presented for the case $M_\infty=10$, $\gamma=5/3$, $Re_\infty=152$, $Pr=\frac{2}{3}$, $T_w=T_\infty$, and no-slip surface conditions. As suggested by Bird,[18] the $u\infty T^{0.5}$ relation represents the correct μ-T relation for a hard-sphere model. In order to show the effect of different μ-T relations on the ML structure, calculations have been carried out for $\mu\alpha T^{0.75}$ and $\mu\alpha T$. In Fig. 8, temperature profiles for cases $\mu\alpha T^{\omega}$ ($\omega=0.5$, 0.75, and 1.0) have been compared with the DSMC calculations.[17] For $\omega=0.5$, we found that the slope of the temperature profile near the wall and maximum temperature agreed reasonably well with those predicted by the DSMC calculations.[17] However, the location of the maximum temperature in the ML zone is different in the two approaches. Also, the continuum approach predicts a much thinner shock-wave-like zone (which may also be called shock wave transition zone) and a shorter tail than those predicted by the DSMC calculations.[17] As ω increases to 0.75 and 1.0, the maximum temperature decreases, its location shifts slightly toward the outside of the ML and the ML thickness increases. In Fig. 9, we have compared the density profiles for the cases $\mu\alpha T^{\omega}$ ($\omega=0.5$, 0.75, and 1.0) with the DSMC predictions of density profile. For $\omega=0.5$, the continuum results show distinctly a shock-wave-like structure, while the DSMC calculations predict a diffused shock wave. Besides, the two profiles are similar near the wall, but differ in magnitude. As ω increases to 0.75 or 1.0, there is no distinct shock-wave-like structure. In Fig. 10, we have plotted the Knudsen numbers based upon the nose radius and the scale length associated with the density gradient.[19] In either case, the mean free path λ is determined by the local fluid properties. Here, $\mu\alpha T^{0.75}$ is taken, but the results are similar where $\mu\alpha T^{0.5}$ is taken. We notice that the nature of the variation of Knudsen numbers from the two definitions is completely different. It is evident that the classical definition of the Knudsen number based upon the nose radius gives physically a plausible variation of the Knudsen number in the ML and approaches the correct asymptotic limit in the freestream.

In Figs. 11-15, we have compared the present results of the structure and overall characteristics of the flow for the Shuttle re-entry conditions with the corresponding results predicted by the DSMC calculations of Moss and Bird.[20] At a 104.93 km altitude, the ML calculations have been carried out for $\gamma=1.31$ using surface slip and temperature jump conditions.

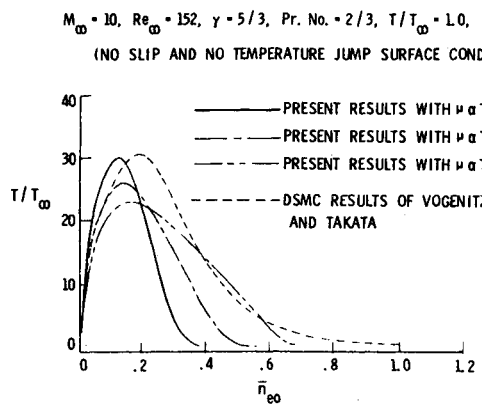

Fig. 8 Comparison of stagnation point temperature profiles with DSMC results.

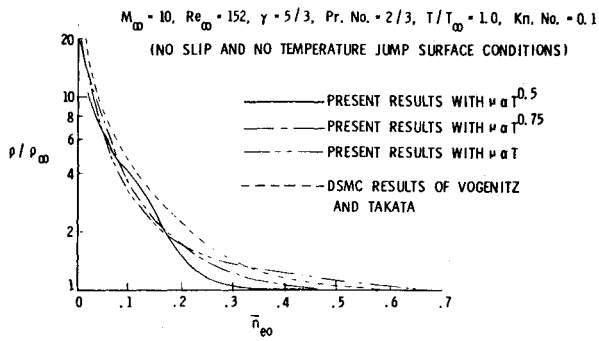

Fig. 9 Comparison of stagnation point density profiles with DSMC results.

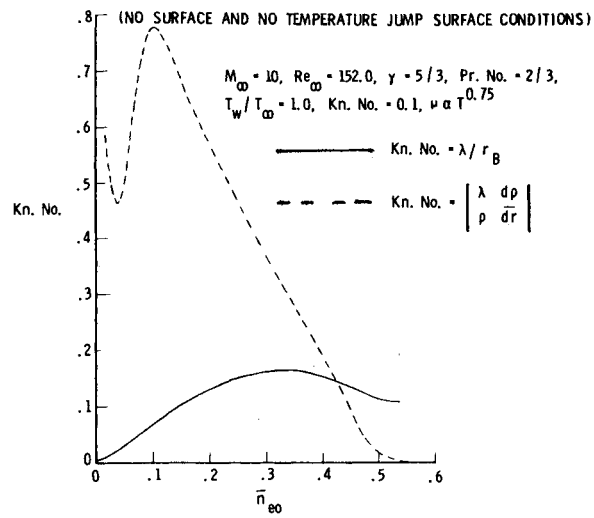

Fig. 10 Variation of stagnation point Knudsen number vs distance from the surface.

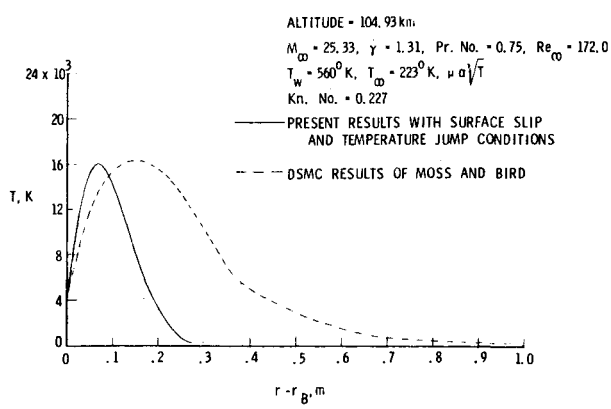

Fig. 11 Comparison of stagnation point temperature profile from the present calculations and DSMC results.

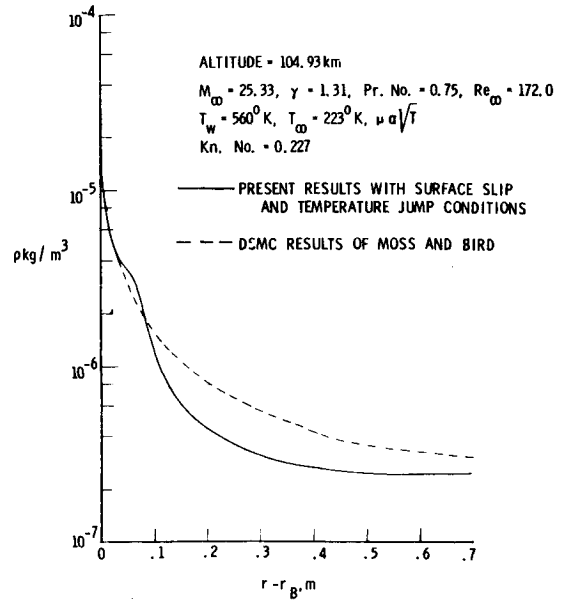

Fig. 12 Comparison of stagnation point density profile with DSMC results.

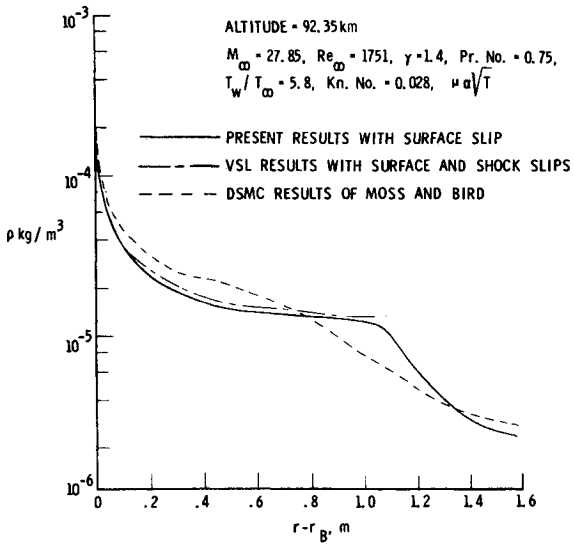

Fig. 13 Comparison of density profiles from the present results and DSMC and VSL calculations.

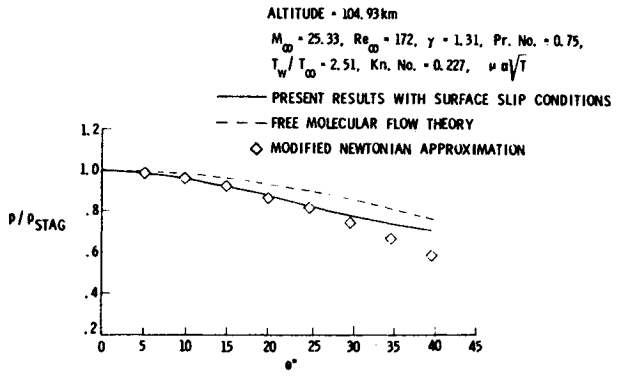

Fig. 14 Comparison of pressure distribution over a sphere with the pressure results of free molecular flow and the modified Newtonian approximation.

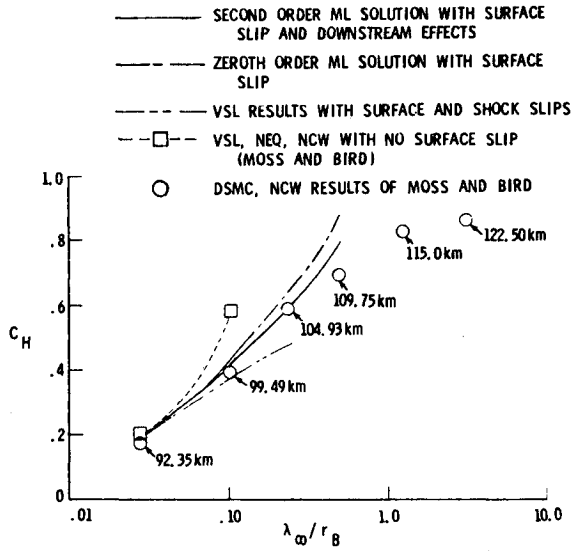

Fig. 15 Comparison of stagnation-point *CH* from present results with VSL and DSMC results.

Moss and Bird[20] pointed out that there was little chemical activity in the flow surrounding the Shuttle beyond 105 km. At 104.93 km altitude, fluid flow around the Shuttle consists of molecular nitrogen and molecular oxygen with partially excited internal degrees of freedom. For air with no vibrational degrees of freedom excited, $\gamma = 1.4$; with rotational and vibrational degrees of freedom fully excited, $\gamma \approx 1.28$. For partially excited vibrational degrees of freedom, we have taken $\gamma = 1.31$ From Fig. 11, we found that the maximum temperature predicted by the ML calculations for $\gamma = 1.31$ agreed reasonably well with the DSMC prediction of maximum temperature. However, the location of the maximum temperature and the structure of the outer layer differ significantly from the two approaches. From Fig. 12, we found that the density profiles from the continuum and the kinetic approaches agreed with reasonable accuracy in the inner layer near the wall. However, in the outer layer away from the wall, the continuum method predicts a shock-wave-like structure, while the kinetic approach predicts no sharp density gradient anywhere in the overlapping region of the inner and outer layers. In Fig. 13, density profiles from the merged-layer calculations with surface slip and viscous shock layer with surface and shock slip[5] are compared with the density profile from DSMC calculations at 92.35 km altitude. We found that the ML and VSL calculations gave slightly differing density profiles. The VSL method predicted the location of a fictitious shock wave of a given strength at almost the same location where sharp gradients in the density profile from the ML method were calculated. Comparing the density profiles from the continnum and kinetic methods, there is reasonable agreement near the wall and significant differences away from the wall. The DSMC method predicts the formation of a shock-wave-like structure much nearer to the wall than predicted by the ML calculations. Figure 14 shows that the surface pressure on the sphere agrees with the modified Newtonian approximation up to $\theta = 30$ deg. This result is in agreement with our findings in Figs. 6 and 7.

In Fig. 15, we have compared the results of stagnation point heat-transfer coefficient C_H for the Shuttle re-entry flight conditions from various continuum calculations with the DSMC calculations of Moss and Bird.[20] Here, the ideal-gas C_H values (with and without downstream effects and surface slip), the VSL results[5] (with surface and shock slip), and the nonequilibrium dissociating VSL results (with no slip and noncatalytic wall[20] are plotted against the rarefaction parameter, the Knudsen number. We found that the results for C_H with downstream effects were in reasonable agreement with the DSMC calculations up to an altitude of 109.75 km. At 92.35

km, although the DSMC calculations show nonequilibrium dissociation in the stagnation point disturbed zone, yet the continuum calculations of C_H for an ideal gas with $\gamma = 1.4$ by different methods agree with the C_H value for a nonequilibrium gas with a noncatalytic wall by DSMC and VSL methods. Species profiles in Figs. 4e and 4f of Ref. 20 show that in the narrow zone near the wall, there is about 76% molecular nitrogen and the rest is atomic oxygen and atomic nitrogen. The molecular oxygen is completely dissociated by the time it reaches the wall. The wall, being noncatalytic and cold, induces little chemical activity in the small region near the wall. Hence, the fluid properties near the wall are primarily determined by the molecular nitrogen that may be represented by an effective value of $\gamma = 1.4$. This may be the reason for little influence of nonequilibrium chemistry on the wall characteristics at the 92.35 km altitude.

Conclusions

The Navier-Stokes equations predicted a thinner shock-wave-like zone with a shorter tail[17,20] than that predicted by the direct-simulation Monte Carlo calculations. From the two approaches, maximum temperature predictions agreed reasonably well in magnitude, but the location of the maximum temperature in the merged layer differed substantially. The present results are similar to the results obtained by Vogenitz and Takata.[17] The capability of the continuum approach to predict shock-wave-like zone has always been in doubt. In view of the very thick shock-wave-like structure in the merged layer regime, which under certain conditions is larger than the viscous layer beneath it, there is need to investigate the question of the validity and accuracy of various approaches in understanding the structure of shock transition zone and its merging with the viscous flow near the surface under hypersonic rarefied conditions. In spite of the discrepancy in the predictions of the continuum and kinetic approaches in the outer portion of the merged layer, continuum results of the surface heat-transfer coefficient C_H agree with the kinetic results with reasonable accuracy up to an altitude of 109.75 km under Shuttle flight conditions.

Acknowledgment

The author expresses his gratitude to Jim J. Jones, Chief, Aerothermodynamics Branch, and James N. Moss, Research Leader, NASA Langley Research Center, for their many helpful suggestions and discussions throughout the research work reported in this paper.

References

[1]Walberg, G.D., "Aeroassisted Orbit Transfer—Window Opens on Missions," *Astronautics and Aeronautics,* Vol. 21, Nov. 1983, pp. 36-43.

[2]Levinsky, F.S. and Yoshihara, H., "Rarefied Hypersonic Flow over a Sphere," *AIAA Progress in Astronautics and Aeronautics: Hypersonc Flow Research,* Vol. 7, edited by F.R. Riddel, Academic Press, New York, 1962, pp. 81-106.

[3]Potter, J.L. and Bailey, A.B., "Pressure in the Stagnation Region of Blunt Bodies in the Viscous Layer to Merged Layer Regimes of Rarefied FLow," AEDC-TDR-63-168, Sept. 1983.

[4]Jain, A.C. and Adimurthy, V., "Hypersonic Merged Stagnation Shock Layers, Part I: Adiabatic Wall Case," and "Part II: Cold Wall Case," *AIAA Journal,* Vol. 12, March 1974, pp. 342-354.

[5]Jain, A.C. and Prabha, S., "A Comparative Study of Stagnation-Point Hypersonic Viscous Shock Layer and Hypersonic Merged-Layer Flows," *Proceedings of 14th International Symposium on Rarefied Gas Dynamics,* edited by H. Oguchi, 1984, pp. 241-248.

[6]Bird, G., "Aerodynamic Properties of Some Simple Bodies in the Hypersonic Transition Regime," *AIAA Journal,* Vol. 4, Jan. 1966, pp. 55-60.

[7]Kumar, A. and Jain, A.C., "Nonequilibrium Merged Stagnation Shock Layers at Hypersonic Speeds," *International Journal of Heat and Mass Transfer,* Vol. 18, 1975, pp. 1113-1118.

[8]Henrick, W.L., "A Similarity Solution of Navier-Stokes Equations with Wall Catalysis and Slip for Hypersonic, Low Reynolds Number Flow over a Sphere," AIAA Paper 75-675, 1975.

[9]Scott, C.D., "An Experimental and Analytical Study of Slip and Catalytic Wall Conditions Applied to Spheres in Low Reynolds Number Arc Jet Flows," *Proceedings of 9th International Symposium on Rarefied Gas Dynamics,* 1974, pp. D.14-1-12.

[10]Davis, R.T., "Numerical Solution of the Hypersonic Viscous Shock-Layer Equations," *AIAA Journal,* Vol. 8, May 1970, pp. 843-851.

[11]Kaiser, J.E. and Flugge-Lots, I., "Viscous, Hypersonic Flow Over a Blunt Body," Stanford University, Stanford, CA, Tech. Rep. 178, Jan. 1968.

[12]Kuo, H.C., "Hypersonic Viscous Flow Near the Stagnation Streamline of a Blunt Body," *AIAA Journal,* Vol. 2, 1964, pp. 1896-1906.

[13]Kennard, E.H., *Kinetic Theory of Gases,* McGraw-Hill Book Co., New York, Indian ed., 1938, pp. 292-298.

[14]Jain, A.C. and Prabha, S., "Hypersonic Second-Order Merged Layers on Blunt Bodies," Dept. of Space, Government of India, Bangalore, Aug. 1982.

[15]Ho, T. and Probstein, R.F., "The Compressible Viscous-Layer in Rarefied Hypersonic Flows," Argonne Research Laboratories, Argonne, IL, Rept. TN-60-132, Aug. 1960.

[16]Boylan, D.E., "Laminar Convection Heat-Transfer Rates on a Hemisphere-Cylinder in Rarefied Hypersonic FLow," *AIAA Journal,* Vol. 9, Aug. 1971, pp. 1661-1663.

[17]Vogenitz, F.W. and Takata, G.Y., "Monte-Carlo Study of Blunt Body Hypersonic Viscous Shock Layers," *Proceedings of 7th International Symposium on Rarefied Gas Dynamics,* pp. 911-918.

[18]Bird, G.A., "Definition of Mean-Free Path in Real Gases," *The Physics of Fluids,* Vol. 26, 1983, pp. 3222-3223.

[19]Bird, G.A., "Low Density Aerothermodynamics," AIAA Paper 85-0994, June 1985.

[20]Moss, J.N. and Bird, G.A., "Direct Simulation of Transitional Flow for Hypersonic Reentry Conditions," AIAA Paper 84-0223, 1984.